Alkali-activated cement sensors for sodium chloride monitoring

L. Biondi, M. Perry, J. McAlorum, C. Vlachakis, A. Hamilton, G. Lo

Abstract

Chloride-induced corrosion of reinforced concrete costs the global economy billions of dollars every year. Despite concerted research effort, the non-invasive, continuous monitoring of sodium chloride in concrete structures is still an unsolved problem. Here, we outline a first-time demonstration of a sodium chloride sensor based on alkali-activated cements: a class of cementitious, electrolytically conductive materials which are typically used for concrete construction and repair. In this work, internal sodium chloride concentrations ranging from 0–22 wt% were measured independently of moisture contents via shifts in electrical impedance. The typical sodium chloride measurement precision was 0.85 wt%. Non-linearity of the sensor response due to signal saturation began at sodium chloride concentrations $>$5 wt%. We use experimental measures of ion dynamics to link this saturation to the deleterious effect of high concentrations on ion mobility. This study demonstrates sensor feasibility, and provides new experimental evidence to further our understanding of ionic conductivity mechanisms in these materials. The work will allow for the development of self-sensing repair and construction materials for locating and quantifying sodium chloride levels within concrete structures — a valuable technology for supporting concrete health monitoring and maintenance.

Index Terms

NaCl sensor, alkali-activated materials, geopolymers, multifunctional materials, smart cements, electrolytic sensors, construction materials.

I. Introduction

Corrosion due to sodium chloride is the leading cause of reinforced concrete degradation [1]–[3], and costs the global economy an estimated $350 bn per year [4]. It is becoming common for corrosion repair costs to exceed initial construction costs, and in the worst cases, poor maintenance has led to complete structural collapse [5]. Sensors for locating and quantifying sodium chloride concentrations within concrete a key aspect of concrete structural health monitoring [6]–[8].

Unfortunately, chloride monitoring is challenging. Some of the most accurate methods we have, such as potentiometric and Volhard methods, are destructive, as they require concrete cores to be extracted from in-service structures [2]. Over the last two decades, an array of non-destructive techniques and sensors have been proposed, including: ion selective electrodes [9]–[14], optical fiber sensors [15]–[17], and in-situ electrical resistivity measurements [18]–[24]. These methods all have their relative advantages, but they all require equipment to be embedded into the concrete structure. This requires a somewhat rare level of foresight during construction, and if the sensors are being retrofitted, holes must be drilled and so techniques are necessarily semi-destructive [9], [25]. Once installed, sensors are typically inaccessible, and so cannot be maintained. Few of these solutions have led to an accepted commercialised product for sodium chloride monitoring in concrete.

The work presented in this paper outlines a first-time demonstration of a new, low-cost sodium chloride sensor technology based on low calcium fly ash alkali-activated materials (AAMs) or cements [26]. Repair and construction materials based on AAMs are an ideal match for concrete structures, because they exhibit similar mechanical, thermal, and moisture transport properties to the more commonly used ordinary Portland cement (OPC) systems. Here, we demonstrate that these proven concrete repair and construction materials [27] can be electrically interrogated and used to monitor changes in their internal sodium chloride concentration. Our methods take advantage of the reasonably high baseline electrolytic conductivity of AAMs [28], [29], so they can be used as sensors without the support of conductive additives.

When used as a repair material, AAM-based sensors could provide distributed surface maps of ionic contamination and moisture levels. We envisage that this surface-level information would be used alongside other non-destructive techniques which assess other important parameters such as the concrete's level of cracking and its porosity. This could allow engineers to assess the overall chloride ingress rate into the structure. If the AAM is used as a construction material (for example as a binder to make concrete, 3D tomographic mapping of impedance may be possible, providing depth information about ion concentrations below the surface. Regardless of the application method, the AAM sensor proposed in this work shows promise

This work was funded in part by the National Nuclear Laboratory ICASE award (NNL/UA/022), EPSRC (EP/L014041/1), the Royal Society (RG160748), and the Scottish Funding Council's Oil & Gas Innovation Centre.

Department of Civil & Environmental Engineering, University of Strathclyde, 75 Montrose Street, Glasgow, G1 1XJ, UK (email: m.perry@strath.ac.uk).

as a retrofittable and replaceable self-sensing repair and construction material. It could benefit the nuclear, transport and off-shore energy generation sectors, all of which have significant inventories of safety-critical coastal-, marine- or de-icing-salt-exposed concrete assets.

II. Theory and Background

AAMs are cementitious repair and construction materials, synthetized by adding an alkaline activator, (in our case, comprised of sodium hydroxide and sodium silicate solution) to raw precursor materials which are rich in aluminium and silicon [26]. Precursors can include blast furnace slag; metakaolin; or fly ash. In the study described here, low calcium fly ash was used as the precursor.

At the time of writing, there are few literature sources to draw from to develop an understanding of AAM ionic conductivity and hence a sensor calibration equation. However, it is known that both AAM and OPC materials have pore solutions that contain electrolytes, and that electrical conduction in these materials stems from ion migration under an applied voltage. A sensor calibration equation can therefore be informed by:

i) literature on ionic conduction mechanisms in AAM and OPC systems;
ii) previous work on electrical resistivity measurements in OPC concretes, and;
iii) our experimental findings, outlined in Section IV.

A. Ionic conductivity changes in the presence of NaCl

AAM and OPC matrix pore solutions both contain electrolytes. Electrical conduction in these materials stems from the migration of anions and cations under an applied voltage. In the AAMs described in this work, the main carriers of ionic current are sodium ions (Na^+) introduced during fabrication of the AAM by the sodium-bearing activator solution. When AAMs are exposed to a sodium chloride (NaCl) solution, additional Na^+ ions, and chloride (Cl^-) ions will also contribute to ionic conductivity. As the quantity of mobile ions in the pore structure increases, so should the ionic conductivity, and we expect this increase to be particularly pronounced when ion mobility is high (e.g. at high moisture contents).

Conductivity gains will, however, saturate at very high sodium chloride concentrations. This is because ion mobility is adversely affected by Coulomb interactions with surrounding ions [30], [31]. At low ionic concentrations, ion motions are mainly limited by their interactions with surrounding solvent molecules.

B. Sensing principle

Environmental parameters can produce measurable shifts in the electrical impedance of an AAM sensing cell. An example cell is shown in Figure 1. If an ac voltage, $V(t)$ is applied to the cell, then the current response, $I(t)$, can be used to calculate the electrical impedance, Z [32]:

$$Z = \frac{V(t)}{I(t)} = Z_{mod}(\cos(\phi) + i\sin(\phi)) = Z_{mod}e^{i\phi}. \tag{1}$$

Here $i = \sqrt{-1}$; $Z_{mod} = |Z|$ is the impedance modulus, the frequency-dependent magnitude of the impedence; and $\phi = arg(Z)$ is the frequency-dependent phase angle between the voltage and current. The electrical resistance of the cell is captured by the real component of the electrical impedance, $Z_{real} = Re(Z)$, while the reactance of the cell is captured by the imaginary component, $Z_{imag} = Im(Z)$. In this study, we assess impedance data using Bode plots (plotting Z_{mod} and ϕ as a function of frequency), and Nyquist plots (plotting Z_{imag} against Z_{real} for all swept frequencies).

Previous work on electrical resistivity measurements of concrete have demonstrated an exponential dependence of resistivity on sodium chloride content, c [18]. Our experimental results, outlined in Section IV, show that this holds true for AAMs, and thus:

$$ln\left(\frac{Z_{mod}}{Z_{mod,0}}\right) = a_1 c + a_2, \tag{2}$$

where $a_{1,2}$ are parametric constants, and Z_{mod} is the impedance modulus at at a particular frequency and NaCl concentration, c [wt %]. Note that c is defined as the concentration of NaCl *inside* the pore solution of the AAM sample, and not the concentration of the surrounding medium. $Z_{mod,0}$ is a baseline impedance modulus, which can be arbitrarily defined using a dry sample in ambient conditions. This normalisation constant is used to eliminate the dependence of the impedance on the geometry of specific AAM samples.

The dependence of the sensor's impedance on moisture content was characterised in our previous work [33], and is described as follows:

$$ln\left(\frac{Z_{mod}}{Z_{mod,0}}\right) = \frac{b_1}{W} + b_2, \tag{3}$$

where $b_{1,2}$ are constants, and W is the water content of the sample [% of open pores filled with water]. Combining equations 2 and 3 results in a characterization equation for moisture and NaCl:

$$ln\left(\frac{Z_{mod}}{Z_{mod,0}}\right) = d_1 + d_2 c + \frac{d_3}{W}, \tag{4}$$

where $d_{1,2,3}$ are constants.

When building a sensor characterisation equation, it is common to include an additional term of the form $d_5 c/W$ to capture any cross-dependence between measurands. However, our experimental results show that there is very little cross-dependence between moisture and NaCl concentration, so the term has been eliminated to maintain simplicity. Equation (4) also fails to capture the non-linear dependence of the sensor at high NaCl concentrations due to the saturation of conductivity gains (as described in Section II-A).

As a result, an equation of the form:

$$ln\left(\frac{Z_{mod}}{Z_{mod,0}}\right) = d_1 + d_2 c + \frac{d_3}{W} + d_4 c^2, \tag{5}$$

provides a better fit with experimental data providing a non-linear term $d_4 c^2$ which captures the saturation of the response over the range of NaCl concentrations tested in this study. All experiments described in this paper were run at a fixed temperature of $T = 20 \pm 1\,^{\circ}$C. A temperature dependence term is therefore not required for characterisation, but could be built in at a later stage by using the characterisation described in our previous work [33].

III. Materials and Methods

A. Sensor fabrication

The sensor developed and tested in this work is shown in Figure 1. The prototype is an AAM sample of dimensions 55 mm × 30 mm × 15 mm, with 4 wire-braided stainless steel electrodes penetrating 2 mm into the corners in a van der Pauw configuration.

The AAM binder was synthesized from low calcium fly ash, using the same materials and methods described in detail in our previous work [33]. The alkaline activator solution was comprised of sodium hydroxide (SH) and sodium silicate (SS) solutions, mixed in a mass ratio of SH/SS = 0.4. The liquid (L=activator solution) to solid (S=fly ash) mass ratio was L/S = 0.5. The AAM cells were cured for 30 days at 20 °C and 95% relative humidity in an environmental chamber prior to testing.

B. Interrogation system

An Electrical Impedance Spectroscopy (EIS) interrogation system was used to apply a 10 mV ac voltage V(t) through the two electrodes shown in Figure 1. The resulting pseudo-linear current response was measured through the remaining two electodes. The frequency of the applied voltage was swept over the range 10 Hz — 100 kHz during impedance characterization.

Within the field of electrochemistry, the application of voltage (rather than current) is known as a potentiostatic measurement. Potentiostatic EIS was chosen as: i) applying a voltage rather than attempting to drive a desired current reduces the risk of electrical breakdown in the cell, and; ii) voltage sources are generally easier to produce than current sources, and so working with applied voltages should streamline any future development of low cost interrogation systems.

C. Calibration procedure

The procedure for the NaCl and moisture calibration is summarized as a flowchart in Figure 2:

1) NaCl solutions of different concentrations (listed in the first column of Table I) were made by dissolving solid NaCl in de-ionised water (Nanopure). Each solution was poured into sealed containers.
2) The AAM cells were removed from the curing environmental chamber, and their initial 'as cured' mass, $M_{i,0}$, was measured.
3) As cured sample cells were placed into empty sealed boxes, housed within a Faraday cage kept at 20 °C, and connected to the interrogation system, in order to measure a baseline impedance value, $Z_{mod,0}$. Impedance spectra were measured five times over a 5 minute duration to allow an average to be taken. These baseline impedance values typically correspond to a water content of $W_{initial} = 77$ ±wt% , a sodium chloride concentration of $c = 0$ wt%, and a temperature of $T = 20 \pm 1\,^{\circ}C$.
4) AAM samples were then soaked in NaCl solutions inside the sealed containers for 24 hours.
5) After soaking, the samples were taken out of the solution, wiped to remove excess solution from the surfaces, and their mass, $M_{i,1}$, was measured.
6) The samples were then sealed in empty boxes for 24 hours to allow the solution inside the pores to equilibrate and homogenise.

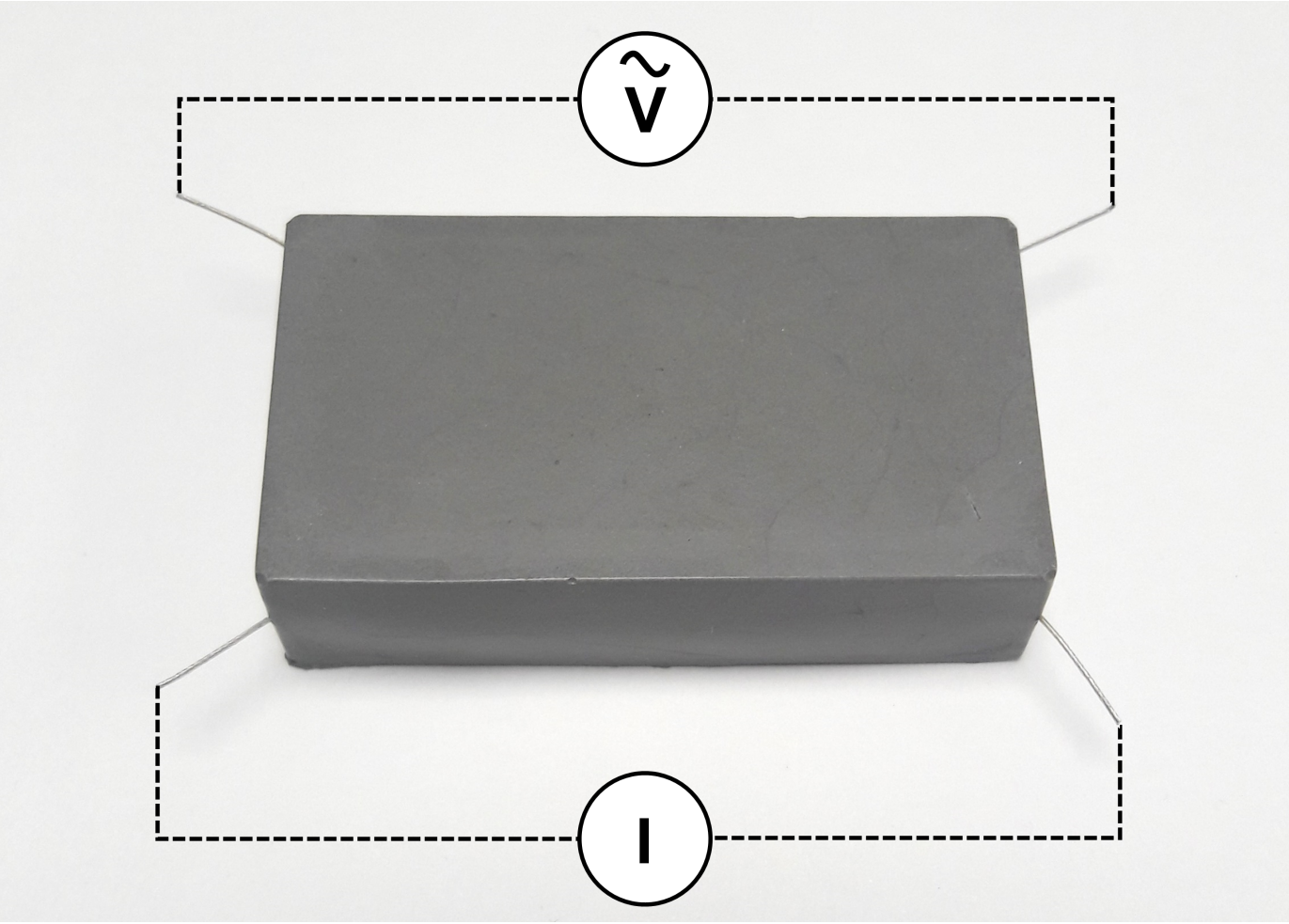

Fig. 1. Photograph of AAM sensor cell showing electrodes used for sensor interrogation.

7) The sealed box containing a sample was placed inside the Faraday cage, and connected to the interrogation system while remaining in the box. Impedance spectra were measured five times and averaged.
8) After the EIS measurement, each AAM sensor was weighed to re-establish its wet mass, $M_{i,2}$. The mass of the sensor M_i was defined as the average of $M_{i,1}$ and $M_{i,2}$. The difference between $M_{i,1}$ and $M_{i,2}$ allowed us to assess the error of our measured moisture content.
9) The AAM sensor was placed in a chamber with silica gel to evaporate water from the sample until a new target moisture content was reached.
10) After all moisture contents had been tested, samples were dried in an oven at 105 °C for 24 hours to establish their dry mass M_d. M_d is the mass of the solid AAM plus the mass of solid NaCl salt inside the sample, $M_d = M_{solid} + M_{salt}$.

To determine the fully saturated mass (i.e. all pores filled) compared to the as-cured or salt solution soaked masses, a separate set of 6 samples were vacuum saturated with de-ionised water after curing, to measure the water saturated mass, $(M_{sat,w})$. This value, an average of the 6 samples, was used to calculate the wt% water content of each sample. The water content (W_s) of samples soaked in NaCl solution is quantified as below. The water content being calculated is the mass of water in the sample at each drying stage divided by the mass of water at full (vacuum) saturation, since saturating by soaking for 24 hours does not fully fill the open pores due to trapped air. The water contents are describing the percentage of available open porosity that has been filled. The same procedure was used in our previous work [33] to calculate water content. In the work presented here, the mass of salt solution (M_{sat}) on the denominator of equations 6 and 7, at pore structure saturation, is calculated from the measured amount of solid salt in the samples after oven drying, and the water saturated mass, $(M_{sat,w})$.

$$W_s = 100 \times \frac{(M_i - M_d)}{(M_{sat} - M_d)} \tag{6}$$

The water content W_i of samples after curing is calculated as:

$$W_i = 100 \times \frac{(M_{i,0} - M_d)}{(M_{sat} - M_d)} \tag{7}$$

A different AAM cell was used for each NaCl concentration value and each repeat measurement. In order to remove the dependence on the specific AAM cell, and to compare the measured values of impedance for different NaCl concentrations, normalized sensor response values $Z_{mod}/Z_{mod,0}$ were generated, as described in Section II-B.

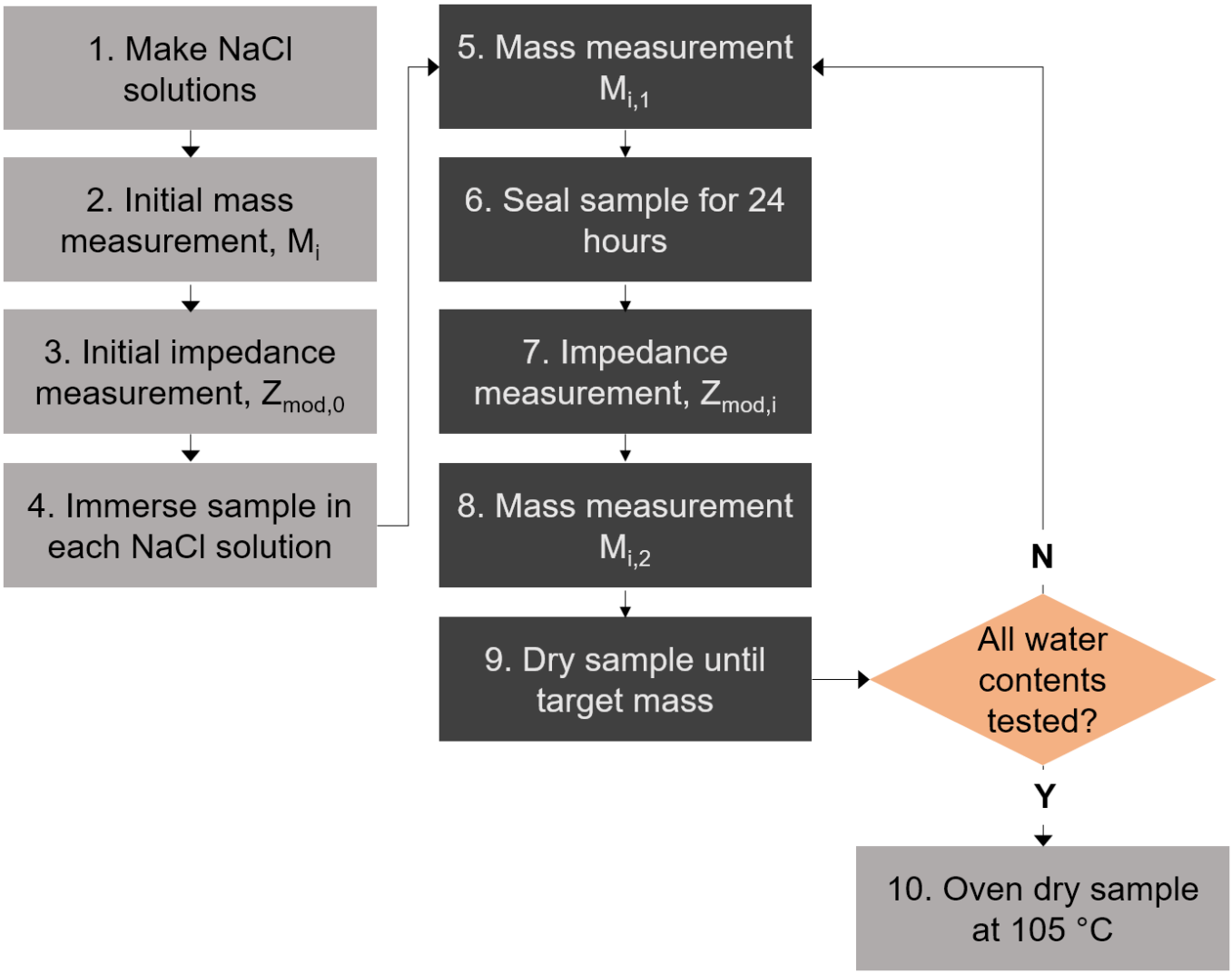

Fig. 2. Flowchart showing the steps in the sodium chloride and moisture characterization experiment.

D. Sodium chloride solutions

Samples were exposed to 10 NaCl solutions, with concentrations ranging from $c_a = 0$ wt % to $c_a = 35.9$ wt %. These concentrations are called the 'applied concentrations', c_a. Note that c and c_a are defined here in wt % as mass of solute/mass of solvent ($\times$ 100) instead of the more standard mass of solute/mass of solution ($\times$100).

After final oven drying (step 10 of the method), the amount of salt remaining in each sample was measured using ion chromatography analysis (IC) Each cell was crushed into a powder, and leached in nanopure water. The water was then analysed using the IC to find the quantity of Cl^- ions leached. This value was used to calculate the actual *internal* sodium chloride concentration, c, within each sample.

The measured mass of salt from the leaching IC analysis, M_{salt}, the mass measurements of the AAM cells after soaking, M_i, and the AAM cell mass after oven drying, M_d, can be used to calculate:

$$c = 100 \times \frac{(M_{salt})}{(M_{wat})} \tag{8}$$

Where M_{wat} is the mass of water inside the AAM cell after soaking in the solution, defined as:

$$M_{wat} = M_i - M_d \tag{9}$$

The uncertainty associated with each actual concentration value, c, is given by the propagation of uncertainty formula:

$$\delta c = c \times \sqrt{\left(\frac{\delta M_{salt}}{M_{salt}}\right)^2 + \left(\frac{\delta M_i}{M_i}\right)^2 + \left(\frac{\delta M_d}{M_d}\right)^2}. \tag{10}$$

The applied NaCl concentration, c_a, and the corresponding actual internal NaCl concentration, c, just after soaking are listed in Table I.

TABLE I

NACL CONCENTRATIONS APPLIED AND CORRESPONDING ACTUAL INTERNAL CONCENTRATIONS IN SAMPLE, EXAMPLES GIVEN FOR INITIAL SOAKING ONLY. ALL WT % VALUES ARE DEFINED AS G SOLUTE/100 G WATER.

Applied NaCl conc. c_a [wt %]	Internal NaCl conc. c [wt %]	
	Value	Error
0	0.002	2E-5
0.49	0.139	8E-4
1.20	0.473	0.003
2.21	0.939	0.006
3.55	1.371	0.008
5.62	2.507	0.015
8.78	3.327	0.020
13.64	5.676	0.034
19.24	10.032	0.064
35.89	15.266	0.103

These additional analysis steps were required because c and c_a are generally not equal. The AAM sample itself contains water prior to soaking, and the leaching of sodium chloride into the sample is a time-dependent process. When deploying these sensors to measure concrete structures in the field in future, knowledge of c will also be more beneficial than knoweldge of c_a, especially if the AAM is bonded to a concrete substrate.

The actual internal NaCl concentrations also change as moisture is evaporated from the samples. This is calculated for each drying point by using equation 8, (but where M_{wat} is the mass of water inside the sample at each drying point), and the corresponding water content is calculated by the gravimetric formula (equation 6). Any removal of solid salt from the pore solution via efflorescence or subflorescence formation during drying over silica gel is not considered in the calculations of pore solution concentration.

IV. RESULTS AND DISCUSSION

A. Impedance dependence on NaCl concentration

Figure 3 and Figure 4 show the typical Bode and Nyquist plots for an AAM sensor cell for the various actual internal NaCl concentration listed in Table I. EIS measurements were all taken at a water content $W = 86 \pm 1$ wt%, and a temperature of $T = 20 \pm 1\,^{\circ}$C. The fits shown in the figures use the same equivalent circuit model described in our previous work [33].

The results show that the AAM cells containing a NaCl solution can still be described by the same circuit models used for AAM cells exposed to pure water. This perhaps should be expected, because the physical AAM matrix itself is not changing: all that is changing is the electrolyte concentration, i.e. the number of Na^+ ions and the presence of Cl^- -ions inside the AAM pore solution. There is therefore no obvious reason why the overall electrochemical description of the system should not remain valid.

Comparing the Z_{mod} values for an AAM sample with no NaCl (shown in [33]) with the Z_{mod} values in Figure 3, shows that the additional NaCl solution improves conductivity. For example, at a frequency of 1 kHz, $Z_{mod}(c = 0) \approx 900$ Ohms and $Z_{mod}(c = 2.7wt\%) \approx 120$ Ohms. Figure 4 also makes it clear that impedance decreases with increasing NaCl concentration, as is expected from the presence of more charge carriers.

B. The role of ion mobility

The data from Figure 4 can be plotted onto a scaled Summerfield plot, as shown in Figure 5. Here, we arbitrarily define a baseline frequency of $f_0 = \omega/2\pi = 100$ Hz, and a baseline admittance taken at 100 Hz of $1/Z_{0,mod} = A_{0,mod} = A_{mod}(100Hz)$ for each line. Further details on how to conduct this process are outlined in [33]. The results found in our work are similar to those found for other brine-saturated porous materials [34].

According to [35], scaled Summerfield plots are only linear if:

$$N_0 q^2 \xi^2 = const, \tag{11}$$

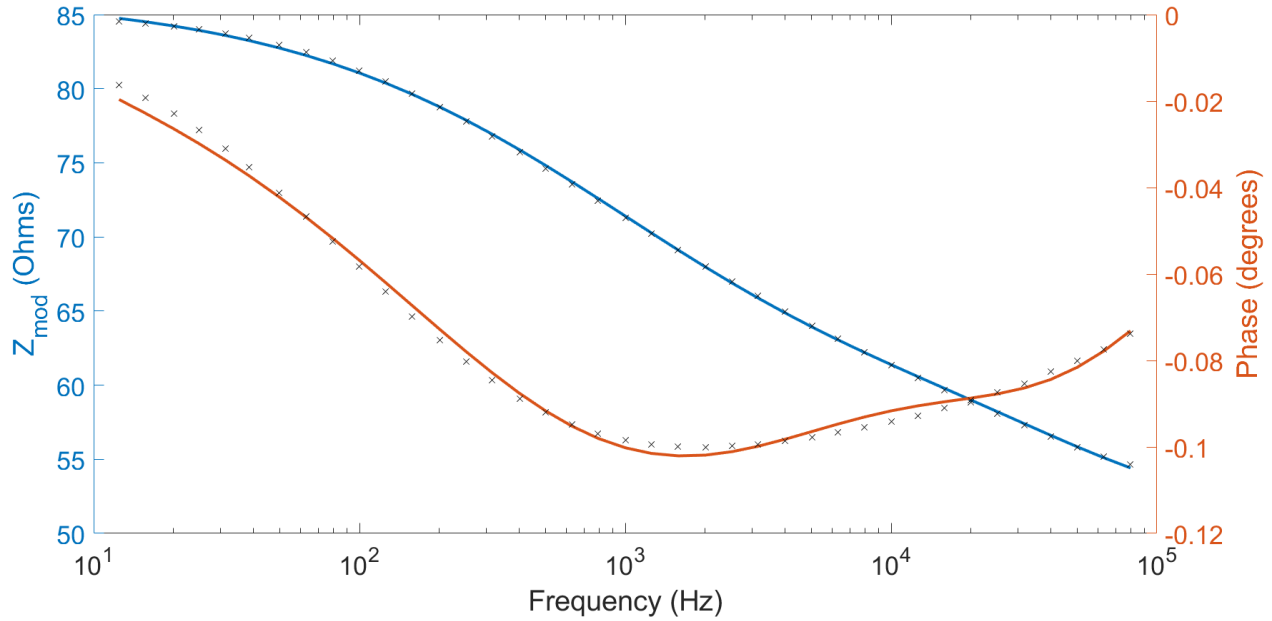

Fig. 3. Typical Bode plots for an AAM sensor cell, taken for an NaCl concentration of $c = 10$ wt%. a water content $W = 86 \pm 1$ wt% and a temperature $T = 20 \pm 1\,\mathrm{deg}$C. The fit uses the equivalent circuit model described in previous work [33].

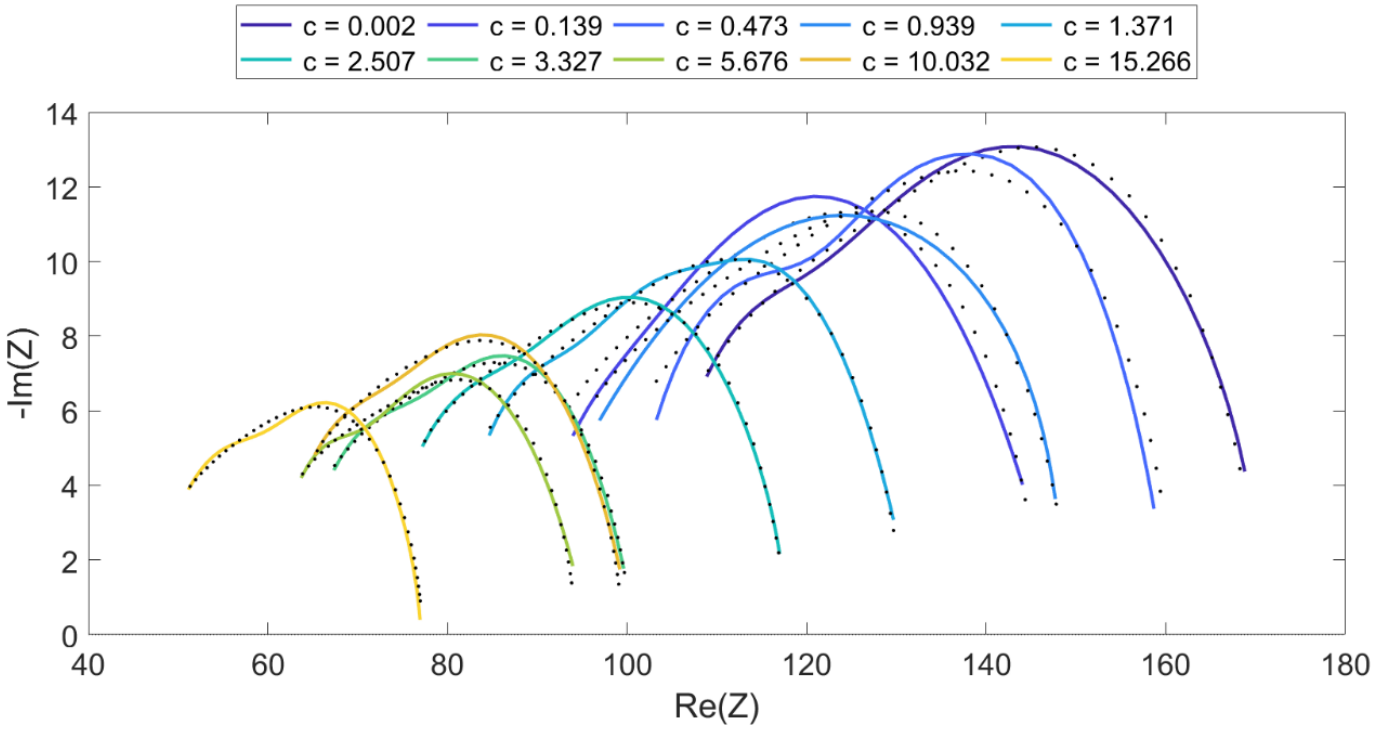

Fig. 4. Nyquist plots from 10 Hz to 100 kHz for various sodium chloride concentrations. Water content $W = 86 \pm 1$ wt% and temperature $T = 20 \pm 1\,\mathrm{deg}$C are constant. Fits use the same equivalent circuit model described in Figure 3.

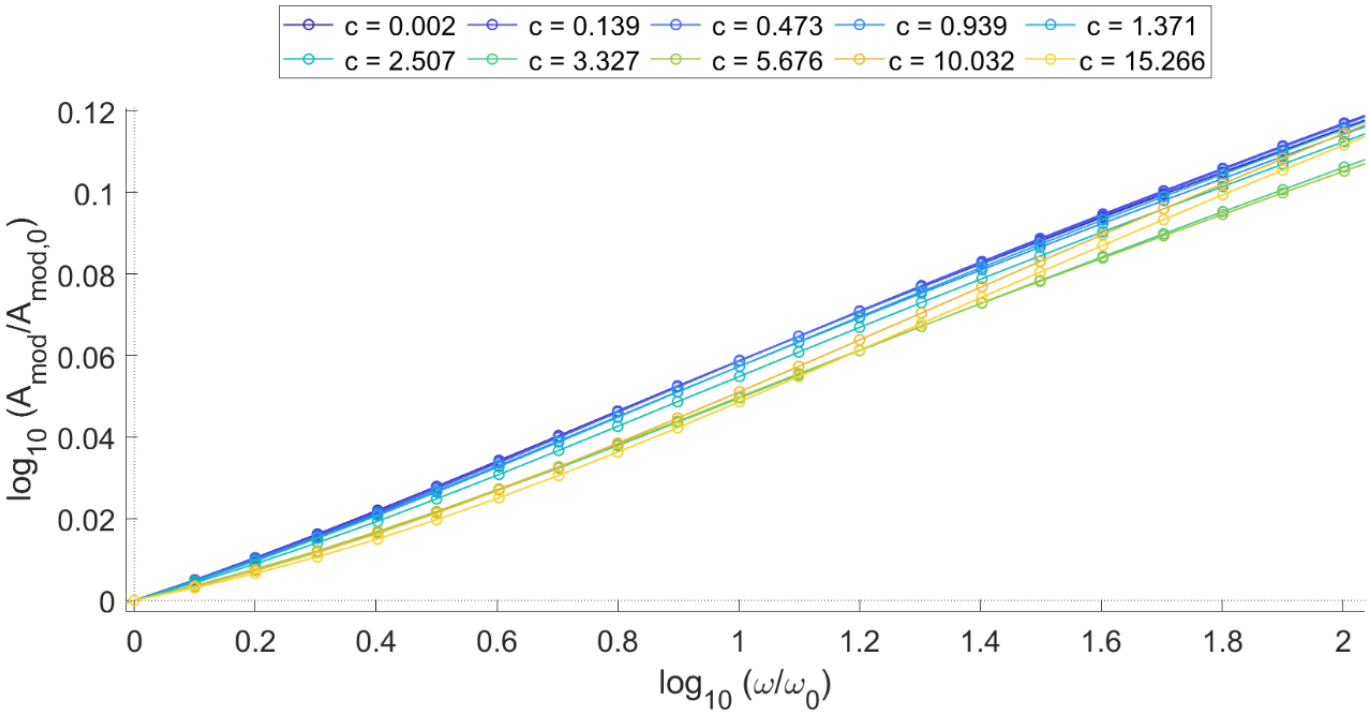

Fig. 5. Scaled Summerfield plots for NaCl as a colorized set of series for each NaCl concentration value, in the range of frequencies from 100 Hz to 10 kHz.

TABLE II
PARAMETERS AND THEIR 95% CONFIDENCE BOUNDS FOR THE SURFACE OF BEST FIT SHOWN IN FIGURE 7 AND DESCRIBED BY EQUATION (4).

	Parameter	d_1	d_2	d_3	d_4
	Value	-2.140	-0.09311	170.2	0.002359
95% confidence	Lower	-2.239	-0.09931	163.4	0.002028
	Upper	-2.041	-0.08690	177.0	0.002689

where N_0 is the total ion concentration in a sample, q is the charge of the ions, and ξ is the diffusion length scale of the ions. It is widely accepted that temperature changes none of these variables (at least over moderate ranges from 5 °C to 30 °C).

The colorization of the data points for each NaCl concentration in Figure 5 shows that there is a change in the proportionality constant of the Summerfield plot as a function of concentration. Previous work in [35] found that changes in the ion concentration of glasses result in a systematic shifting in the proportionality constant of scaled Summerfield plots. In glasses, this was linked to the fact that the distance ions must hop to reach vacant sites changes as a function of N_0. A similar mechanism linking the ion concentration to the availabilty of vacant sites could be responsible for the results shown here for alkali-activated materials.

Figure 5 also shows that the curves corresponding to the highest concentrations ($c > 9$ wt%), tend to superimpose onto the lowest concentration curves ($c < 1.37$ wt%). Mathematically at least, this implies that the quantity $N_0 q^2 \xi^2$ takes a similar value at particularly high and low sodium chloride concentrations. The underlying mechanisms responsible for this particular result are however unclear, and further work is required.

Figure 6 shows the sensor response to sodium chloride concentration for samples at a constant water content of $W = 86 \pm 1$ wt% and constant temperature of $T = 20 \pm 1\,°C$. The interrogation frequency is constant, at 1 kHz. This frequency was chosen as it is achievable with most affordable electronics, and as shown by Figure 3, it corresponds to a region where phase angles tend to have a maximised magnitude: in other words, we are assessing shifts in the peak of the Nyquist plots shown in Figure 4, in an attempt to increase sensitivity.

As shown, equation (2) provides a good fit to the data. The data points further from the curve can be attributed to experimental noise in temperature, water content values, or sodium chloride concentrations.

The overall response of the sensor for any general water / NaCl concentration combination is better characterized by fitting moisture and NaCl simultaneously, as shown in Figure 7. In this figure, we have defined the inverse of a sample's moisture content as the 'dryness' of the sample, $1/W$. Equation (4) is an excellent fit for water contents between W =60 wt% and W = 86wt%. The parameters of the nonlinear fit and their 95% confidence bounds are provided in Table II, and the data points are explictly listed in Table IV.

A reality that Figure 7 fails to capture is that the sodium chloride concentration within a sample will itself be dependent on changes in moisture content. It is therefore possible to completely remove the water content dependence from the data shown

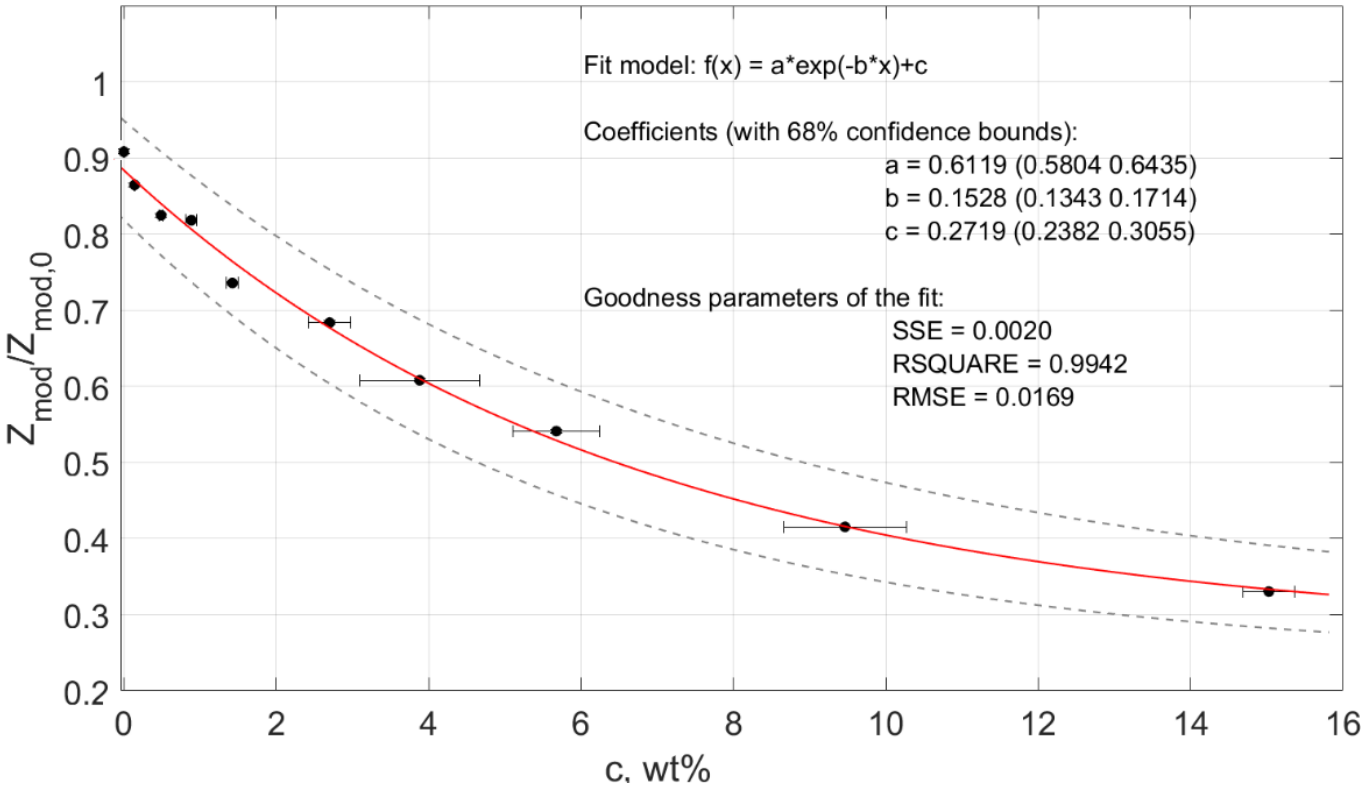

Fig. 6. Normalised shift in impedance as a function of NaCl concentration.

TABLE III
PARAMETERS AND THEIR 95% CONFIDENCE BOUNDS FOR THE LINE OF BEST FIT SHOWN IN FIGURE 8.

	Parameter	d_5	d_6	d_7
95% confidence	Value	0.5940	0.1730	0.3655
	Lower	0.5656	0.1506	0.3363
	Upper	0.6225	0.1953	0.3946

in Figure 7, and instead express all data points on a sodium chloride concentration axis. This mapping can be done because each stage of drying can instead be viewed as increasing the sodium chloride concentration within the pores of the sample. Any efflorescence or subflorescence of salt crystals is not being considered here. Efflorescence was only visible in the samples with the highest sodium chloride concentration used.

Recalculation of the concentration by accounting for moisture loss results in the plot shown in Figure 8. The new normalised impedance values are fit using a similar equation to (2), that is:

$$Z_{modNorm_w} = d_5 e^{(-d_6 c)} + d_7. \tag{12}$$

The parameters of this fit and their confidence intervals are given in Table III.

When deployed in future work, the response of the AAM sensor to internal NaCl concentration could be separated from its response to moisture, with the use of a second 'reference sensor'. This reference sensor could be a sensor which is insensitive to NaCl, or an AAM sensor which is not exposed to NaCl. The reference sensor's moisture readings could be used to compensate for water response in the AAM sensor using an equation of the form:

$$c = -\frac{1}{b_2} ln\left(\frac{Z_{modnorm_w} - b_3}{b_1}\right) \tag{13}$$

The datapoints in Figure 8 do deviate from the line of best fit in some regions, but most points are within the 95% confidence bounds. Fluctuations are mostly attributable to the summation of errors during the process of mapping drying stages to sodium chloride concentrations.

C. Sensor precision

The sensor's NaCl measurement precision was calculated by mapping the impedance fluctuations of the EIS interrogator onto the NaCl concentration axes. This could be done using the calibration curve shown in Figure 8.

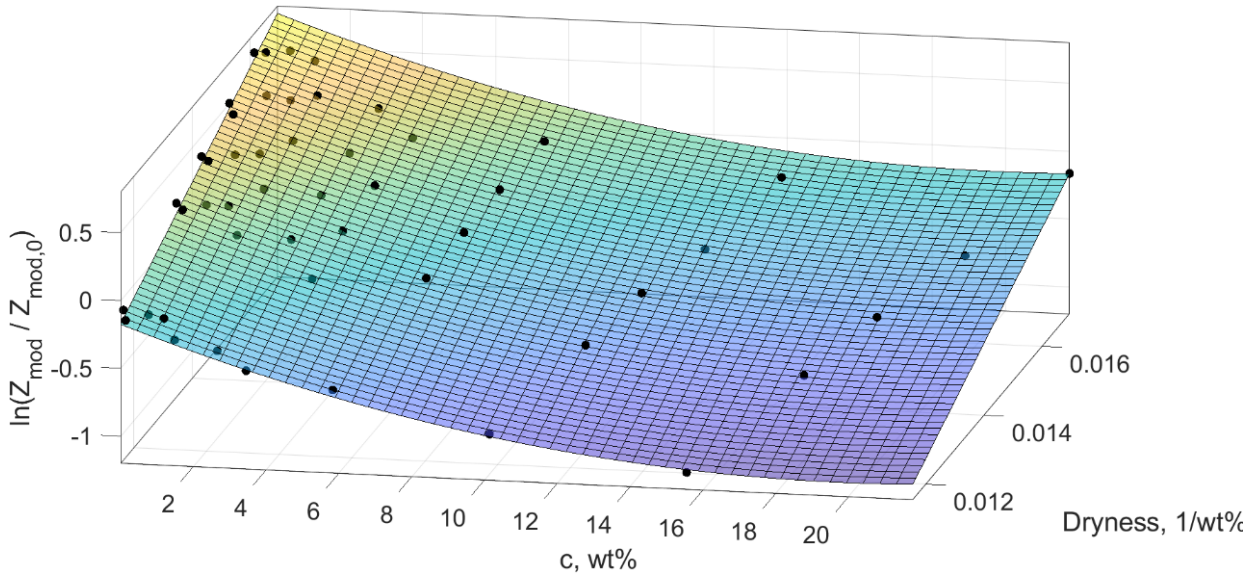

Fig. 7. 3D plot of sensor calibration curve for dryness (the inverse of moisture content), and NaCl concentration.

The AAM sensor's response is not linear over broad ranges of NaCl concentration. This means that sensor precision is not a constant. The fractional errors in $Z_{modNorm_w}$ are in the range 0.01 – 0.04 %. This error is comprised of the direct measurement errors in Z_{mod}, and also the errors in the interpolation process for water content compensation.

Following this exercise, we found that typical sensor precision is $\delta c = 0.85$ wt%. The worst case precision of $\delta c = 5.84$ wt% occurs in the region where the sensor response is saturated, and the best case precision of $\delta c = 0.21$ wt% corresponds to low concentrations, $c < 1$ wt %, where the sensor shows a higher sensitivity.

D. Challenges for future work

Sodium chloride is one of the most common salts that concrete structures are exposed to, but in-service structures can be exposed to several other harmful salts such as sulphates dissolved in ground water and calcium and magnesium chlorides used in de-icing salts. Any other salts would likely change the electrical impedance of an AAM layer or structure. As part of future work, and prior to application of this technology in the field, the sensor's ability to selectively sense these ions will need to be characterised. We may find that different salts cause different and even frequency-dependent changes in the electrical impedance response. If this is the case, then characteristic equations can be built to distinguish between ions. Alternatively, a reference sensing scheme could be developed, with the AAM providing distributed overall map of ion contamination alongside point sensing from ion selective electrodes. Changes to the composition of the AAM, or the addition of secondary coatings, to capture or reduce specific ion migration, are other avenues worth investigating in future work.

A second point which may require further investigation is the alkali-silica reaction (ASR) that could occur within AAM concrete, or within an OPC concrete structure instrumented with an AAM surface-repair. ASR could potentially cause long-term drifts in the sensor's response or gradual degradation of the underlying concrete. The risk of this in our present work is probably low because: i) the low-calcium fly ash AAM used in this study has been associated with a lower risk for ASR [36], and; ii) the low thickness of our coatings means the total inventory of mobile alkalis to cause ASR is low. Nevertheless, further studies are required to explicitly assess whether ASR is caused by AAMs in contact with existing concretes, whether it is a localised or time-constrained effect, and whether mitigating changes to the deployment process or AAM chemistry are required to ensure long-term reliability for the sensor and substrate.

V. Conclusions and Future Work

We have demonstrated the viability of using alkali-activated cements to monitor sodium chloride contamination. Our experimental campaign characterized the impedance response of alkali-activated material cells for fifty internal NaCl concentrations ranging from 0 wt% – 22 wt%. This range of NaCl concentrations covers the exposure of concrete to low levels of contamination up to a severe cases of contamination (a saturated NaCl solution).

The results show that changes in NaCl concentration inside the pore solution of the sensor cell result in changes in impedance, with an exponential dependence. The calibration equation found in previous work for the impedance dependence on moisture was confirmed to hold for all cases of NaCl contamination. The performance of our sensors makes them particularly suitable for monitoring sodium chloride concentrations below 5 wt%. Beyond this point, the sensor response begins to gradually saturate. For context, the concentration of seawater is around 3–4 wt%.

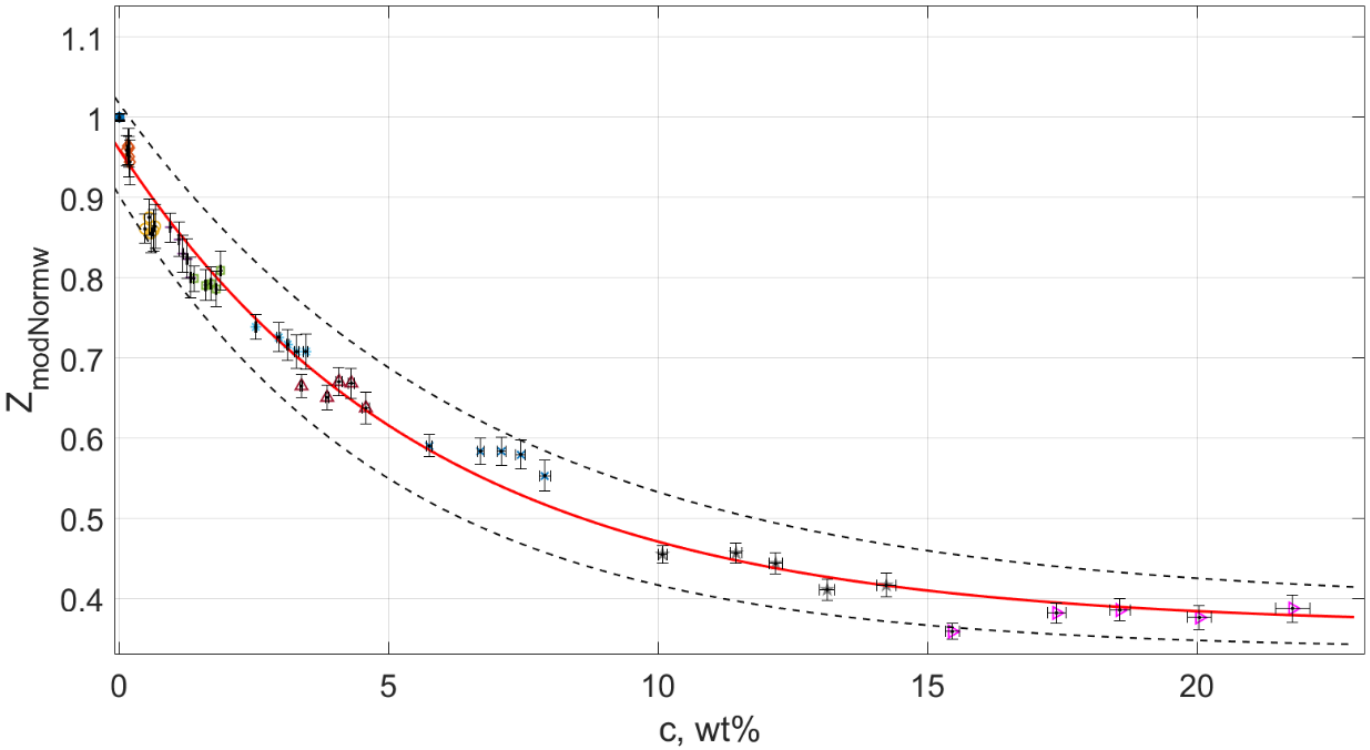

Fig. 8. Final calibration curve for sensor response as a function of sodium chloride content, with moisture dependence removed.

Future work will focus on a more complete calibration, that takes into consideration temperature effects for each moisture and sodium chloride contamination level, and investigates the impact of other common ions on electrical impedance. We will also explore the response of the material when it is applied as a repair to a conventional concrete substrate. A repeatability evaluation, and measurements of system drift and dynamic response will also be required before the sensors can be deployed in the field.

ACKNOWLEDGMENT

Thank you to Dr Tatyana Peshkur for technical support during analysis of ion leaching, and to Dr Carmelo Mineo for assistance with programming for data analysis.

REFERENCES

[1] F. P. Glasser, J. Marchand, and E. Samson, "Durability of concrete—Degradation phenomena involving detrimental chemical reactions," *Cem. Concr. Res.*, vol. 38, no. 2, pp. 226–246, 2008.
[2] M. Torres-Luque, E. Bastidas-Arteaga, F. Schoefs, M. Sánchez-Silva, and J. F. Osma, "Non-destructive methods for measuring chloride ingress into concrete: State-of-the-art and future challenges," *Const. Build. Mater.*, vol. 68, pp. 68–81, 2014.
[3] C. Andrade, M. Castellote, and R. d' Andrea, "Measurement of ageing effect on chloride diffusion coefficients in cementitious matrices," *J. Nucl. Mater.*, vol. 412, no. 1, pp. 209–216, 2011.
[4] G. Koch, J. Varney, N. Thompson, O. Moghissi, M. Gould, and J. Payer, "NACE International Impact Report: International Measures of Prevention, Application, and Economics of Corrosion Technologies Study," Tech. Rep., 2016.
[5] M. F. Montemor, A. M. P. Simoes, and M. G. S. Ferreira, "Chloride-induced corrosion on reinforcing steel: From the fundamentals to the monitoring techniques," *Cem. Concr. Compos.*, vol. 25, no. 4-5, pp. 491–502, 2003.
[6] H. S. Lee, M. A. Ismail, J. K. Singh, and J. H. Shin, "Embedded sensor system to detect chloride permeation in concrete: An overview," *Corros.*, vol. 52, no. 5, pp. 373–382, 2017.
[7] R. E. Melchers and C. Q. Li, "Phenomenological modeling of reinforcement corrosion in marine environments," *ACI Materials Journal*, vol. 103, no. 1, p. 25, 2006.
[8] G. K. Glass and N. R. Buenfeld, "Chloride-induced corrosion of steel in concrete," *Progress in Structural Engineering and Materials*, vol. 2, no. 4, pp. 448–458, 2000.
[9] B. Elsener, L. Zimmermann, and H. Böhni, "Non destructive determination of the free chloride content in cement based materials," *Materials and Corrosion*, vol. 54, no. 6, pp. 440–446, 2003.
[10] C. P. Atkins, M. A. Carter, and J. D. Scantlebury, "Sources of error in using silver/silver chloride electrodes to monitor chloride activity in concrete," *Cem. Concr. Res.*, vol. 31, no. 8, pp. 1207–1211, 2001.
[11] C. P. Atkins, J. D. Scantlebury, P. J. Nedwell, and S. P. Blatch, "Monitoring chloride concentrations in hardened cement pastes using ion selective electrodes," *Cem. Concr. Res.*, vol. 26, no. 2, pp. 319–324, 1996.
[12] G. S. Duffó and S. B. Farina, "Development of an embeddable sensor to monitor the corrosion process of new and existing reinforced concrete structures," *Const. Build. Mater.*, vol. 23, no. 8, pp. 2746–2751, 2009.
[13] G. S. Duffó, S. B. Farina, and C. M. Giordano, "Characterization of solid embeddable reference electrodes for corrosion monitoring in reinforced concrete structures," *Electrochimica Acta*, vol. 54, no. 3, pp. 1010–1020, 2009.

TABLE IV
DATA SET OF CHLORIDE CONCENTRATION, DRYNESS AND SENSOR RESPONSE VALUES.

c [wt%]	Dryness [1/wt%]	Sensor response, $ln(Z_{mod}/Z_{mod,0})$
0	0.0116	-0.0964
0	0.0135	0.2278
0	0.0143	0.3528
0	0.0153	0.5021
0	0.0161	0.6563
0.500	0.0115	-0.1455
0.583	0.0135	0.1779
0.621	0.0143	0.3179
0.658	0.0152	0.4459
0.705	0.0163	0.6202
1.199	0.0119	-0.1928
1.389	0.0138	0.135
1.484	0.0147	0.2668
1.587	0.0158	0.4398
1.665	0.0166	0.5739
2.181	0.0118	-0.2007
2.552	0.0139	0.1154
2.730	0.0149	0.2536
2.905	0.0158	0.4046
3.044	0.0166	0.5014
3.394	0.0117	-0.3069
3.933	0.0135	-0.0091
4.165	0.0144	0.1266
4.415	0.0152	0.2611
4.624	0.016	0.41
5.404	0.0117	-0.3804
6.314	0.0137	-0.0667
6.680	0.0145	0.0537
7.030	0.0153	0.1696
7.384	0.0161	0.2995
8.403	0.0116	-0.4977
9.577	0.0133	-0.2435
10.119	0.0141	-0.0854
10.682	0.0149	0.0457
11.344	0.0159	0.1564
12.793	0.0116	-0.6142
14.890	0.0137	-0.2928
15.728	0.0145	-0.1585
16.521	0.0153	-0.037
17.504	0.0162	0.0765
17.596	0.0116	-0.8786
19.825	0.0132	-0.6126
21.206	0.0142	-0.4754
22.531	0.0152	-0.3904

[14] G. De Vera, M. A. Climent, C. Antón, A. Hidalgo, and C. Andrade, "Determination of the selectivity coefficient of a chloride ion selective electrode in alkaline media simulating the cement paste pore solution," *J. Electroanal. Chem.*, vol. 639, no. 1-2, pp. 43–49, 2010.

[15] P. L. Fuhr and S. J. Spammer, "Fiber optic sensors in the Waterbury bridge," vol. 3489. International Society for Optics and Photonics, 1998, pp. 124–129.

[16] J.-L. Tang and J.-N. Wang, "Measurement of chloride-ion concentration with long-period grating technology," *Smart Mater. Struct.*, vol. 16, no. 3, p. 665, 2007.

[17] C. C. C. Lam, R. Mandamparambil, T. Sun, K. T. Grattan, S. V. Nanukuttan, S. E. Taylor, and P. M. Basheer, "Optical fiber refractive index sensor for chloride ion monitoring," *IEEE Sens. J.*, vol. 9, no. 5, pp. 525–532, 2009.

[18] M. Fares, G. Villain, S. Bonnet, S. P. Lopes, B. Thauvin, and M. Thiery, "Determining chloride content profiles in concrete using an electrical resistivity tomography device," *Cem. Concr. Compos.*, vol. 94, pp. 315–326, 2018.

[19] W.-J. Park, H.-S. Lee, S.-H. Joh, and H.-S. Lee, "Monitoring method for the chloride ion penetration in mortar by a thin-film sensor reacting to chloride ion," *Const. Build. Mater.*, vol. 53, pp. 403–410, 2014.

[20] W. J. McCarter and O. Vennesland, "Sensor systems for use in reinforced concrete structures," *Const. Build. Mater.*, vol. 18, no. 6, pp. 351–358, 2004.

[21] W. J. McCarter, T. M. Chrisp, G. Starrs, A. Adamson, E. Owens, P. A. M. Basheer, S. V. Nanukuttan, S. Srinivasan, and N. Holmes, "Developments in performance monitoring of concrete exposed to extreme environments," *J. Infrastruct. Syst.*, vol. 18, no. 3, pp. 167–175, 2011.

[22] R. B. Polder, "Test methods for on site measurement of resistivity of concrete—a RILEM TC-154 technical recommendation," *Const. Build. Mater.*, vol. 15, no. 2-3, pp. 125–131, 2001.

[23] R. B. Polder and W. H. Peelen, "Characterisation of chloride transport and reinforcement corrosion in concrete under cyclic wetting and drying by electrical resistivity," *Cem. Concr. Compos.*, vol. 24, no. 5, pp. 427–435, 2002.

[24] P. A. M. Basheer, P. R. V. Gilleece, A. E. Long, and W. J. Mc Carter, "Monitoring electrical resistance of concretes containing alternative cementitious materials to assess their resistance to chloride penetration," *Cem. Concr. Compos.*, vol. 24, no. 5, pp. 437–449, 2002.

[25] R. Prakash, "Non-destructive testing of composites," *Composites*, vol. 11, no. 4, pp. 217–224, 1980.

[26] J. L. Provis, "Geopolymers and other alkali activated materials: Why, how, and what?" *Materials and Structures*, vol. 47, no. 1, pp. 11–25, Jan. 2014.

[27] F. Pacheco-Torgal, J. Castro-Gomes, and S. Jalali, "Alkali-activated binders: A review: Part 1. Historical background, terminology, reaction mechanisms and hydration products," *Const. Build. Mater.*, vol. 22, no. 7, pp. 1305–1314, 2008.
[28] S. Hanjitsuwan, P. Chindaprasirt, and K. Pimraksa, "Electrical conductivity and dielectric property of fly ash geopolymer pastes," *Int. J. Miner. Metall. Mater.*, vol. 18, no. 1, pp. 94–99, 2011.
[29] X.-M. Cui, G.-J. Zheng, Y.-C. Han, F. Su, and J. Zhou, "A study on electrical conductivity of chemosynthetic Al2O3–2SiO2 geoploymer materials," *Journal of Power Sources*, vol. 184, no. 2, pp. 652–656, 2008.
[30] R. A. Robinson and R. H. Stokes, *Electrolyte Solutions*. Courier Corporation, 2002.
[31] J. Bisquert, V. Halpern, and F. Henn, "Simple model for ac ionic conduction in solids," *J. Chem. Phys.*, vol. 122, no. 15, 2005.
[32] A. Lasia, "Electrochemical impedance spectroscopy and its applications," in *Modern Aspects of Electrochemistry*. Springer, 2002, pp. 143–248.
[33] L. Biondi, M. Perry, J. McAlorum, C. Vlachakis, and A. Hamilton, "Geopolymer-based moisture sensors for reinforced concrete health monitoring," *Sens. Actuators B Chem.: Chemical*, vol. 309, p. 127775, 2020.
[34] A. Ramsamugh and F. Brouers, "Scaling law for the low-frequency ac conductivity of fluid-saturated porous media," *Philosophical magazine letters*, vol. 55, no. 6, pp. 301–304, 1987.
[35] D. L. Sidebottom, "Colloquium: Understanding ion motion in disordered solids from impedance spectroscopy scaling," *Rev. Mod. Phys.*, vol. 81, pp. 999–1014, Jul 2009. [Online]. Available: https://link.aps.org/doi/10.1103/RevModPhys.81.999
[36] W. Wang and T. Noguchi, "Alkali-silica reaction (ASR) in the alkali-activated cement (AAC) system: A state-of-the-art review," vol. 252, p. 119105. [Online]. Available: https://www.sciencedirect.com/science/article/pii/S0950061820311107